Three-phase borate solid solution with low sintering temperature, high quality factor, and low dielectric constant: Experimental and DFT study

Rui Peng[a], Hua Su[a,b,*], Yuanxun Li[a,*] Yongcheng Lu[a], Liang Shi[a], Wei Du[a], Xiaoli Tang[a], Guoliang Yu[c], Minshu Chen[d],

[a] State Key Laboratory of Electronic Thin Films and Integrated Devices, University of Electronic Science and Technology of China, Chengdu 610054, China

[b] Jiangxi Guochuang Industrial Park Development Co., Ltd, Ganzhou 341000, China.

[c] China Jiliang University, Hangzhou 310018, China.

[d] Nanjing University of Information Science and Technology, Nanjing 210000, China.

[*] e-mail: uestcsh77@163.com, liyuanxun@uestc.edu.cn

Abstract

The sintering and microwave dielectric properties of a ceramic material based on Mg^{2+} substituted $Zn_3B_2O_6$ have been widely studied using first principles calculations and experimental solid-state reactions. Characterization methods include the Network Analyzer, X-ray, Raman diffraction, scanning electron microscopy, energy-dispersive spectroscopy, and differential-thermal & thermo-mechanical analyzer. The increasing amount of Mg^{2+} results in the appearance of $Mg_2B_2O_5$ and ZnO, and the mutual substitution (Mg^{2+} and Zn^{2+}) phenomenon has emerged in $Zn_3B_2O_6$ and $Mg_2B_2O_5$. The mechanisms have been explained with the help of DFT calculations. The bond parameters and electron distributions of the ZnO_4 tetrahedron and the MgO_6 octahedron have been modified due to substitution. The sintering, substitution, and phase formation properties have been analyzed quantitatively through the energy parameters. The best dielectric properties were obtained for x=0.20 sintered at 950°C,

ε_r=6.47, $Q\times f$=89,600GHz (15.2GHz), τ_f=-48.6ppm/°C, relative density=96.7%. The substitution of Mg^{2+} to Zn^{2+} is a feasible method to improve the microwave dielectric properties of the $Zn_3B_2O_6$ ceramic.

Keywords: LTCC; Dielectric properties; DFT; Borate; Solid solutions

1. Introduction

Low temperature co-fired ceramics (LTCC) technology has attracted significant research interest recently due to its ability of large scale three-dimensional integration with passive devices. For the inner electrode, the maximum processing temperature of LTCC is the melting point of Ag (961°C).[1] The materials used in the field of microwave communication require both low dielectric constant (ε_r) and high quality factor ($Q\times f$).[2] Hence, considering both the electrical characteristics of the material and the processing temperature, the ceramic with low ε_r, high $Q\times f$, and low densification temperature has great potential application value in the field of LTCC.[3,4]

Ceramic material based on $Zn_3B_2O_6$ (ZBO) has recently been studied in the context of batteries and luminescence, but studies on the sintering and microwave dielectric properties of ZBO are less common.[5,6] Wu *et al.* reported that the ZBO ceramic demonstrated good dielectric properties when sintered at 925°C, *i.e.*, ε_r=6.7, $Q\times f$=58, 500GHz, τ_f =-58ppm/°C, and relative density=96%.[7] While the dielectric constant and the sintering temperature of ZBO ceramic are acceptable, the $Q\times f$ value can be improved. Dosler *et al.* have found that the dielectric properties of the $Mg_3B_2O_6$ (MBO) ceramic are ε_r=7, $Q\times f$=108,000GHz, τ_f =-69ppm/°C, and relative density=97% sintered at 1350°C.[8] Considering that the $Q\times f$ value of MBO is larger than that of ZBO, and the densification temperature of ZBO is smaller than that of MBO, we speculate that the addition of MBO into ZBO is a possible way to

synthesize a composite ceramic with both low densification temperature and high $Q\times f$ value without the increasing the ε_r.

The composite ceramic, (1-x)ZBO+xMBO (x=0.00-0.40), was synthesized through the solid-state reaction method. The analysis of microstructure, sintering property, and microwave dielectric properties is included in the discussion. Additionally, the first principle calculation based on the density functional theory (DFT) was used to provide theoretical interpretations.

2. Experimental procedures

The raw materials, ZnO, MgO, and B_2O_3, of analytical purity, were from Chron Chemicals Co. Ltd., Chengdu, China. According to the stoichiometric ratio (10 mol% excess of B_2O_3 for the compensation), these powders were pre-milled for 12h, pre-sintered at 850℃ for 4h and milled again for 12h. The medium of milling was distilled water and agate balls. The resulting powders were mixed with the polyvinyl alcohol binder (5wt%), pressed into disks (6mm in thickness and 12mm in diameter), and sintered at 900-1000℃.

The Cambridge Serial Total Energy Package (CASTEP) was used to perform the first principles calculation, and the Vanderbilt ultrasoft pseudopotential was adopted to approximate the interaction of ions and electrons. The exchange-correlation interaction was approximated through the Perdew-Burke-Ernzerhoff function. The linear response method was used to calculate the vibration of atoms. The configuration of the valence electrons was taken as $3d^{10}4s^2$ for Zn, $2p^63s^2$ for Mg, $2s^22p^4$ for O, and $2s^22p^1$ for B. After testing, the parameter of the energy cutoff and the k-point mesh were set as 375eV and 4×4×3, respectively. Other parameters include 0.01eV/Å (maximum force), 0.02GPa (maximum stress), 5.0×10^{-6}eV/atom (total energy), 5.0×10^{-6}eV/atom (energy), and

0.005Å (maximum displacement). The optimization of geometry was obtained using the Broyden-Fletcher-Goldfarb-Shanno algorithm. The substituted system was constructed based on a relaxed super cell (1×2×2, 176 atoms), and the formation energy was obtained using Eq. 1,[9]

$$\Delta E = E_{Do} - E_{UnDo} - \sum_i k_i p_i \tag{1}$$

where E_{Do} and E_{UnDo} are the total energy of the doped cell and un-doped cell, p_i represents the chemical potentials of the substituted atom, and k_i represent the unite coefficient.

X-ray diffraction (XRD: DX-2700, Haoyuan Co.) with Cu K_α radiation was used to measure the crystal data of samples, which were processed using the Rietveld profile refinement method. The microstructure and the elemental composition were confirmed with the help of scanning electron microscopy (SEM: JEOL, JSM-6490LV) and energy-dispersive X-ray spectroscopy (EDS). Based on the transmission cavity method and the Hakki-Coleman method, the microwave dielectric properties were obtained through the Agilent N5230A Network Analyzer (300MHz-20GHz).[10] The sintering property was investigated by the thermo-mechanical analyzer (TMA: Mettler TMA/SDTA2+) and simultaneous thermal analyzer (TGA&DSC: Mettler TGA/DSC3+). The temperature coefficient of resonant frequency (τ_f) was obtained from Eq. 2 using the resonant frequency at 80℃ (f_T) and 20℃ (f_0),[11]

$$\tau_f = \frac{f_T - f_0}{f_0 (T - T_0)} \times 10^6 \tag{2}$$

The Archimedes method was used to measure the bulk density.[12] The theoretical τ_f, ε_r, and Q values were calculated with the mixing rule,[13-15]

$$\tau_f = v_a \times \tau_{fa} + v_b \times \tau_{fb} \tag{3}$$

$$\ln \varepsilon_r = v_a \ln \varepsilon_{ra} + v_b \ln \varepsilon_{rb} \tag{4}$$

$$\frac{1}{Q} = \frac{v_a}{Q_a} + \frac{v_b}{Q_b} \tag{5}$$

where $v_{a(b)}$ is the volume fraction of phase a(b); $\tau_{fa(b)}$, $\varepsilon_{ra(b)}$ and $Q_{a(b)}$ are the dielectric properties of phase a(b). The activation energies (E_a) were calculated using the Arrhenius expression,[16]

$$\ln k = \frac{-E_a}{R}\left(\frac{1}{T}\right) + \ln z \tag{6}$$

where R (8.3145J/K/mol) is the gas constant, k is the heating rate (5, 10, and 15K/min), T is the temperature (Kelvin), and z is Arrhenius constant.

3. Results and discussion

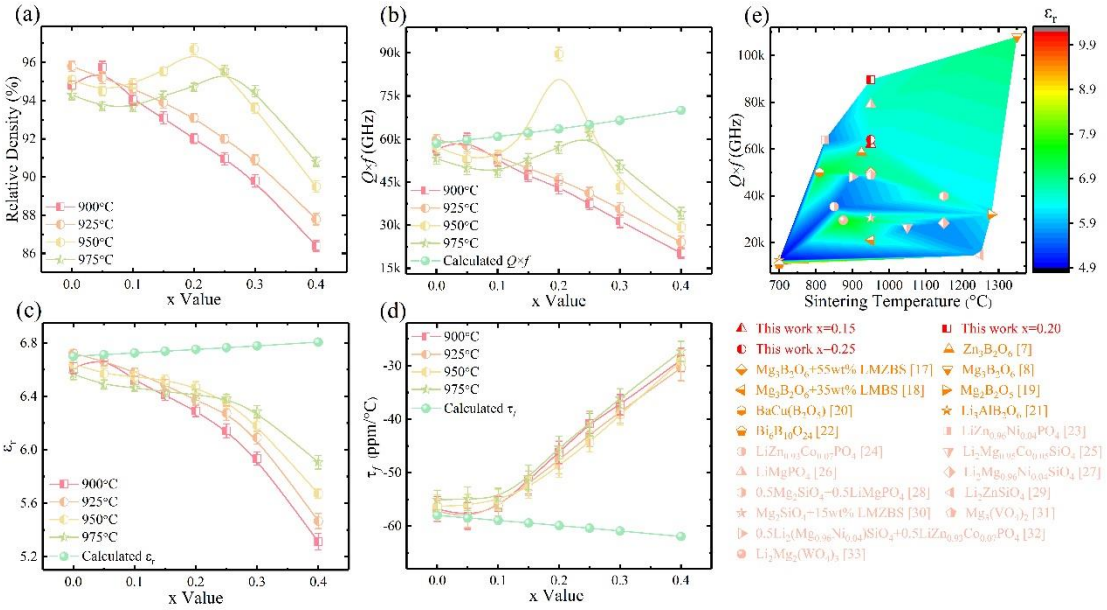

Fig. 1 Relative density (a), $Q\times f$ (b), ε_r (c), and τ_f (d) values of the (1-x)ZBO+xMBO (x=0.00-0.40) ceramics sintered at different temperature; summary of sintering and dielectric properties of various ceramics (e)

Fig. 1(a-d) present the dielectric properties of the (1-x)ZBO+xMBO ceramics sintered at different temperatures. The relative density value shows a trend of (i) first increasing and then decreasing for samples sintered at 900°C, (ii) monotonous decreasing for samples sintered at 925°C, and (iii) wavy for

the one sintered at 950 and 975℃. The peak density value was 96.7% for the sample with x=0.20 sintered at 950℃. The variation trend that the $Q\times f$ value presents is in accordance with that of the relative density, and it peaked at x=0.20, 89,600GHz at 15.2GHz, which can be attributed to the strong interdependence between these two parameters. As x increases, the ε_r value shows a monotonously decreasing trend, except for the sample sintered at 900℃, which shows a parabolic trend, and ε_r=6.47 as x=0.20 sintered at 950℃. The relative density variation could be one reason for the variation of the ε_r value since the sample with a high level of densification shows a relatively high ε_r value and samples with low density show low ε_r values. The τ_f value shows an overall increasing trend with τ_f=-48.6ppm/℃ for x=0.20 sintered at 950℃. Therefore, a moderate addition of Mg^{2+} improved the densification level, $Q\times f$ value, and thermal stability while decreasing the ε_r value of the ZBO ceramic. As shown in Fig. 1(e), the composite ceramics synthesized in this experiment provided both excellent dielectric and sintering properties when compared with other ceramics.[7, 8, 17-33]

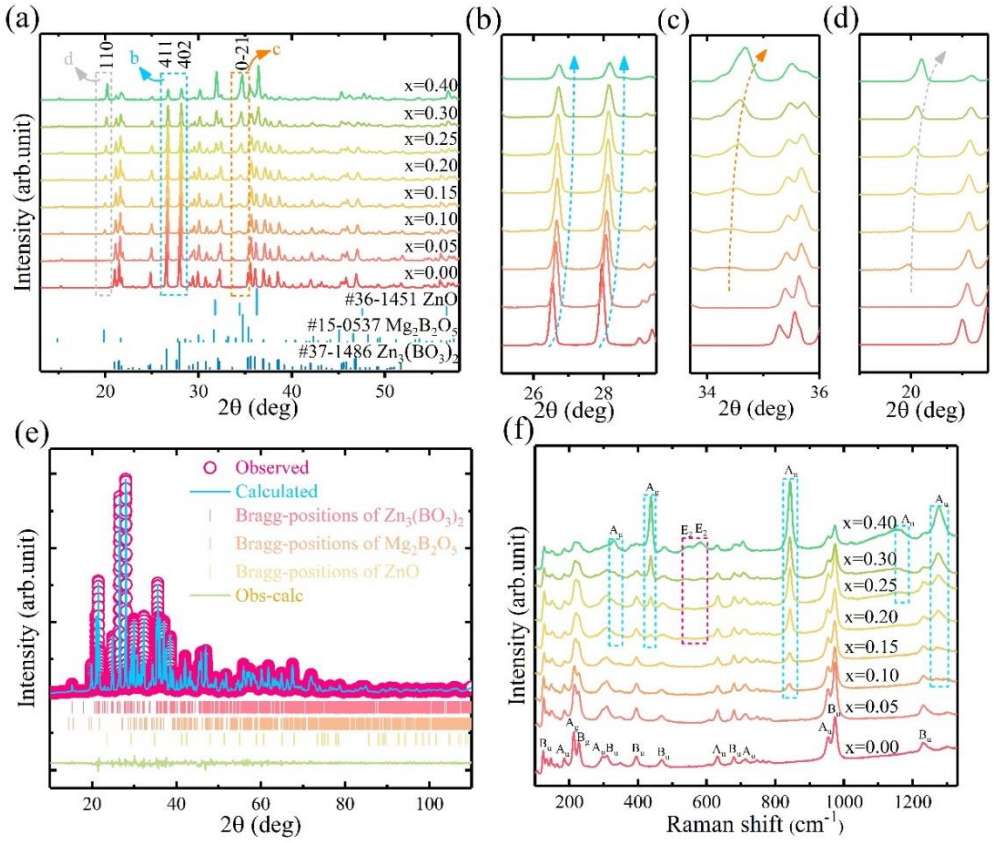

Fig. 2 XRD patterns of the (1-x)ZBO+xMBO (x=0.00-0.40) ceramics sintered at 950℃ (a-d); experimental and calculated profiles of the 0.8ZBO+0.2MBO ceramic sintered at 950℃ (e); Raman spectroscopy of the (1-x)ZBO+xMBO (x=0.00-0.40) ceramics sintered at 950℃

Fig. 2(a-d) presents the XRD patterns of all the samples processed at the same temperature (950℃). A single ZBO phase (JCPDS#37-1486) was formed for the samples with x=0.00 and 0.05 and increasing the Mg^{2+} content resulted in the emergence of the $Mg_2B_2O_5$ phase (JCPDS#15-0537) and the ZnO phase (JCPDS#36-1451). The peak intensity of ZBO was seen to decrease, and that of $Mg_2B_2O_5$ and ZnO increased as the x value increased. The (411) and (402) peaks of the ZBO ceramic and the (110) and (0-21) peaks of the $Mg_2B_2O_5$ ceramic shifted to a higher angle, indicating that the cell volume of both the ZBO ceramic and the $Mg_2B_2O_5$ ceramic decreased on increasing Mg^{2+}-ions. Considering that the ionic radius of Zn^{2+} (0.60Å) was larger than that of Mg^{2+}

(0.57Å) and that the Mg^{2+} concentration increased with increase in the x value, the ion substitution level of Mg^{2+} to Zn^{2+} (ZBO ceramic) could have strengthened, and that of Zn^{2+} to Mg^{2+} ($Mg_2B_2O_5$ ceramic) could have weakened, thus, explaining the variation in volume.[34] The detailed lattice parameters obtained from refinement are provided in Fig. 2e, Table I, and Fig. 3. The theoretical, calculated, and measured values match well; the Fullprof parameters are satisfactory. For the ZBO ceramics, parameters a, c, and the volume tend to decrease; b and β increase; and α and γ remain unchanged. For the $Mg_2B_2O_5$ ceramic, parameters a, b, c, and the volume tend to decrease, while α, β, and γ increase. The variation of lattice parameters is consistent with the observations from the XRD data. It should be noted that both the formed component and component fraction is different from the designed one. The designed fraction value of the ZBO ceramic is smaller than that measured for $x \leq 0.20$, and the designed value exceeds the measured value when $x > 0.20$. The mutual ion substitution, *i.e.*, Mg^{2+} to Zn^{2+} for ZBO ceramic and Zn^{2+} to Mg^{2+} for $Mg_2B_2O_5$ ceramic, and the formation of ZnO ceramic can explain this discrepancy. The fraction of $Mg_2B_2O_5$ and ZnO ceramic increased with the addition of Mg^{2+} when $x \geq 0.10$. Since the densification temperature of ZBO is 925℃, the increasing density for the sample with x=0.05 sintered at 900℃ should be attributed to the decreasing densification temperature due to lattice distortion, and the decreasing density value for the same sample sintered at 925-975℃ can be ascribed to the over-sintering. The decreasing density of samples sintered at 900, and 925℃ is a result of the formation of $Mg_2B_2O_5$, which has a densification temperature of about 1280℃.[19] The increment of density for samples sintered at 950 and 975℃ can be attributed to the reduction in the extent of over-sintering, and any subsequent decrease is the same as that of the sample sintered at a lower temperature. Since the $Mg_2B_2O_5$ ceramic has a relatively lower ε_r (6.2) and higher τ_f (-18ppm/℃) compared to that of the ZBO ceramic, the formation of a heterophase can explain

the difference between the measured and calculated ε_r/τ_f value except for the density level variation.[19] However, the $Q\times f$ value of the composite ceramic with x=0.20 sintered at 950℃ is larger than that of both ZBO and $Mg_2B_2O_5$ (32,100GHz at 12.6GHz) ceramic.[19] These phenomena can be explained by the modification of the crystal structure led by mutual substitution, the formation of a solid solution with three phases, and the improved density level. Furthermore, the existence of the ZnO phase also has an impact on the sintering and dielectric properties of the composite ceramics.

The Raman spectra of all samples were obtained to further study phase formation, as shown in Fig. 2(f). According to the Bilbao Crystallographic Server and CASTEP, the vibration modes for ZBO, $Mg_2B_2O_5$, and ZnO ceramics are as follows,

$$\Gamma_{Optic} = 33A_g(R) + 32A_u(IR) + 33B_g(R) + 31B_u(IR) \tag{7}$$

$$\Gamma_{Optic} = 27A_g(R) + 24A_u(IR) \tag{8}$$

$$\Gamma_{Optic} = A_1(IR\,\&\,R) + 2B_1(R) + 2E_2(R) + E_1(IR\,\&\,R) \tag{9}$$

where R corresponds to the Raman mode, and IR corresponds to the Infrared mode. Considering the testing error due to the peak overlap, sample shape, and temperature of the test environment, the peaks obtained from the experiment and calculation fitted well. For the sample with pure ZBO phase (x=0.00), the vibration modes at the frequency lower than 503cm^{-1} were the external modes (rotational and translational modes of ZnO_4), and the other half were the internal modes (bending and stretching vibration modes of BO_3). The increasing value of x is seen to result in the weakening of peaks belonging to ZBO and the enhancement of other peaks; the formation of $Mg_2B_2O_5$ (blue dashed box) and ZnO (pink dashed box) phases could be the reason for such a variation.[35] The dividing point of external and internal modes for $Mg_2B_2O_5$ ceramic is 740cm^{-1}. The external modes involve the rotational and translational modes of MgO_6, and the internal modes are the same as the ZBO ceramic.

Therefore, the discussion regarding the phase composition obtained from XRD can be confirmed by the Raman spectra.

Table I. Refinement and lattice parameters of the (1-x)ZBO+xMBO (x=0.00-0.40) ceramics by the Rietveld profile refinement method

Parameters	x=0.00	x=0.05	x=0.10	x=0.15	x=0.20	x=0.25	x=0.30	x=0.40
R_p (%)	5.14	6.02	6.24	6.35	6.41	6.37	5.56	5.91
R_{wp} (%)	5.92	6.12	6.89	7.16	7.29	7.48	7.22	7.31
R_{exp} (%)	5.01	5.21	5.85	6.17	6.20	6.28	5.36	5.44
χ^2	1.40	1.38	1.39	1.35	1.38	1.42	1.81	1.81

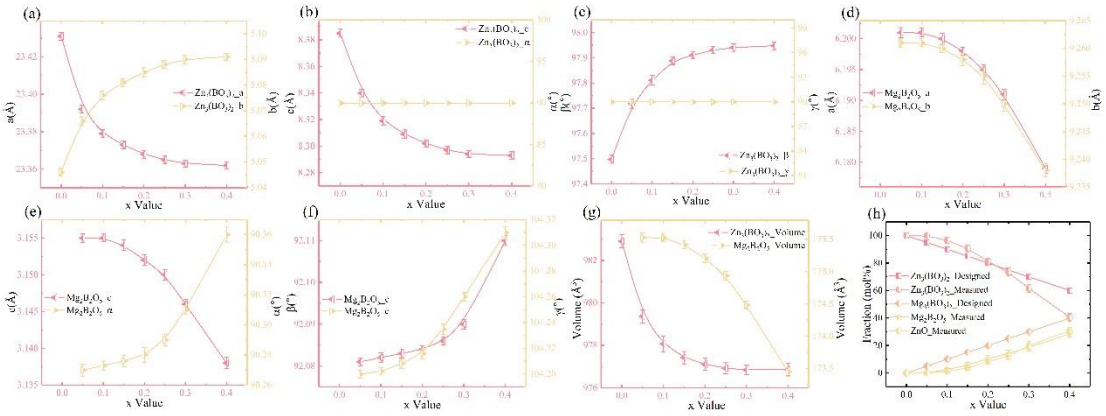

Fig. 3 Lattice parameters of ZBO and $Mg_2B_2O_5$ ceramics sintered at different temperature

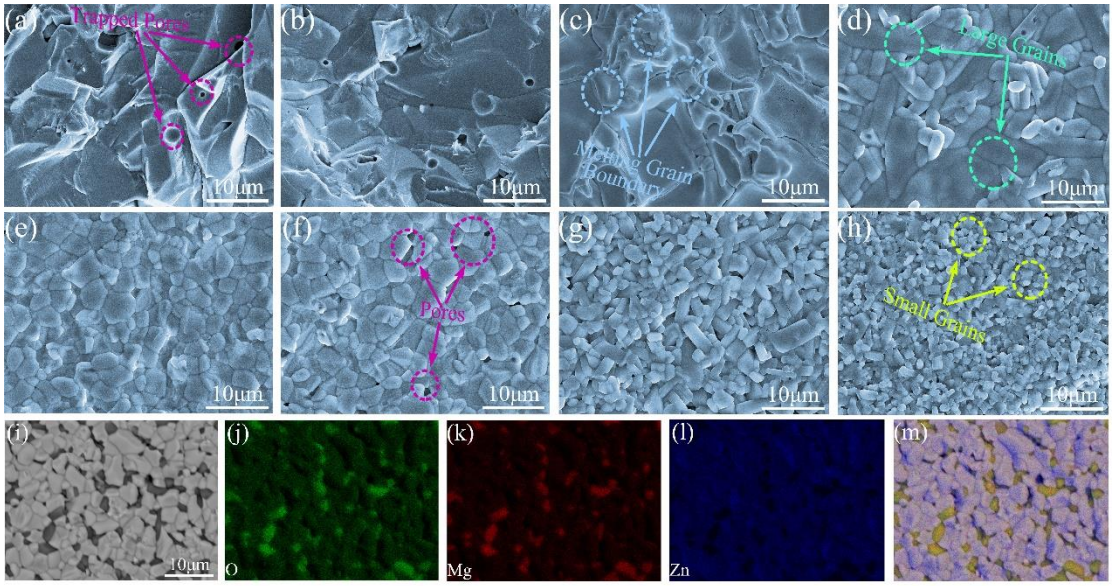

Fig. 4 SEM micrographs of the (1-x)ZBO+xMBO (x=0.00-0.40) ceramics sintered at 950℃ (a-h);

EDS mapping images of the 0.8ZBO+0.2MBO ceramic sintered at 950℃ (i-m)

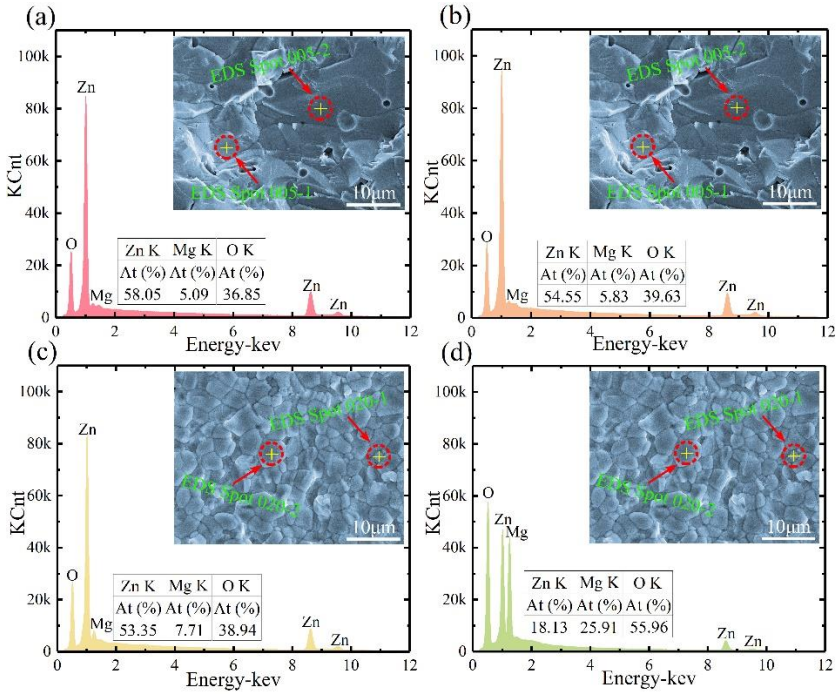

Fig. 5 EDS result of the (1-x)ZBO+xMBO (x=0.00-0.40) ceramics as x=0.05 (a, b) and x=0.20 (c, d)

sintered at 950℃

The microstructure of the samples sintered at 950℃ is shown in the SEM images in Fig. 4. The trapped pores (pink circles) and melting grain boundaries (blue circles) are observed in Fig. 4(a-c), and abnormal grain growth is observed in Fig. 4(d) which is scattered with large grains (green circles). A compact microstructure is obtained in the sample with x=0.20, and any further addition of Mg^{2+} leads to the reduction of grain size (yellow circles) and the emergence of pores (pink circles) at the same sintering temperature. The behavior observed from the SEM images fits well with the relative density trends observed. Fig. 4(i-m) show the EDS mapping of the sample with x=0.20, where the distribution of oxygen, zinc, and magnesium are shown to be uneven. The O-rich grains are also Mg-rich, and the other grains which are Zn-rich relatively lack O. The relationship between the zinc and magnesium content is in accordance with the design one generally. EDS was conducted to confirm the composition of the composite materials (x=0.05, x=0.20) sintered at 950℃, as shown in Fig. 5. All elements were detected except for boron (too light). The atomic ratio of Zn: Mg: O is 58.05: 5.09: 36.85 for spot 005-1, 54.55: 5.83: 39.63 for spot 005-2, 53.35: 7.71: 38.94 for spot 020-1, and 18.13: 25.91: 55.96 for spot 020-2. The EDS result for x=0.05 sample is consistent with the designed value, demonstrating that no second phase was generated and that the ZBO phase was distributed uniformly. However, this two mole ratio values of Zn: Mg: O for the x=0.20 sample was different, and the content of various elements was different from different grains. The grain at spot 020-1 tested Zn-rich and the grain at spot 020-2 was O&Mg-rich, which is consistent with the result from EDS mapping. Therefore, the EDS results confirmed the observations made from XRD regarding the phase formation.

In order to analyze the sintering property of the (1-x)ZBO+xMBO (x=0.00-0.40) ceramics, TG, DSC and TMA were conducted (Fig. 6(a-c)). The temperature increase from 100℃ to 300℃ led to a weight loss of about 11%. The first stage of weight loss can be ascribed to the removal of hydration

water, and the decomposition of H_3BO_3 (formed from the reaction of B_2O_3 and distilled water). The further decomposition of H_3BO_3 could be responsible for the second stage of gradual weight loss (slight) from 300℃ to 600℃. After that, the dynamic atom equilibrium was achieved, and the negligible weight loss was observed for temperatures higher than 600℃. The DSC curves show an endothermic peak at around 200℃, corresponding to the first stage of weight loss. The exothermic peak near 610℃ can be ascribed to the crystallization of the ZBO ceramic and the further decomposition of H_3BO_3. The exothermic peak at a relatively higher temperature (blue dotted box) could be attributed to the formation of $Mg_2B_2O_5$, which corresponds to further weight loss near 680℃ (blue dotted box). It should be noted that the increasing Mg^{2+} content shifts the weight loss and endothermic peak near 200℃ to a lower temperature, and also shifts the exothermic peak for the formation of ZBO ceramic to a relatively higher temperature. The TMA patterns show that the onset point of shrinkage move to a higher temperature, which matches the observations from the TG and DSC. Hence, the addition of Mg^{2+} led to a slightly higher temperature window of densification of the ZBO ceramic, and the heterophase was formed with a relatively high *x* value. The activation energy was calculated at the temperature where 3%, 6%, and 9% shrinkage was observed to further investigate the sintering properties. The *lnk* versus *1/T* plots are shown in Fig. 6(d-k).[36] Calculations (Fig. 6(l)) show that the E_a value tends to decrease and then increase. The initial decrease of E_a demonstrates that the lattice distortion (led by 5% Mg^{2+} substitution) could lower the densification temperature of ZBO ceramic as discussed in context to the relative density. The followed increase in E_a verifies that the heterophase could indeed increase the densification temperature of the composite ceramic at $x \geq 0.10$. Specifically, the sample with the addition of 5% Mg^{2+} had the lowest E_a (407±183kJ/mol), and the E_a value for x=0.20 sample was 598±221kJ/mol.

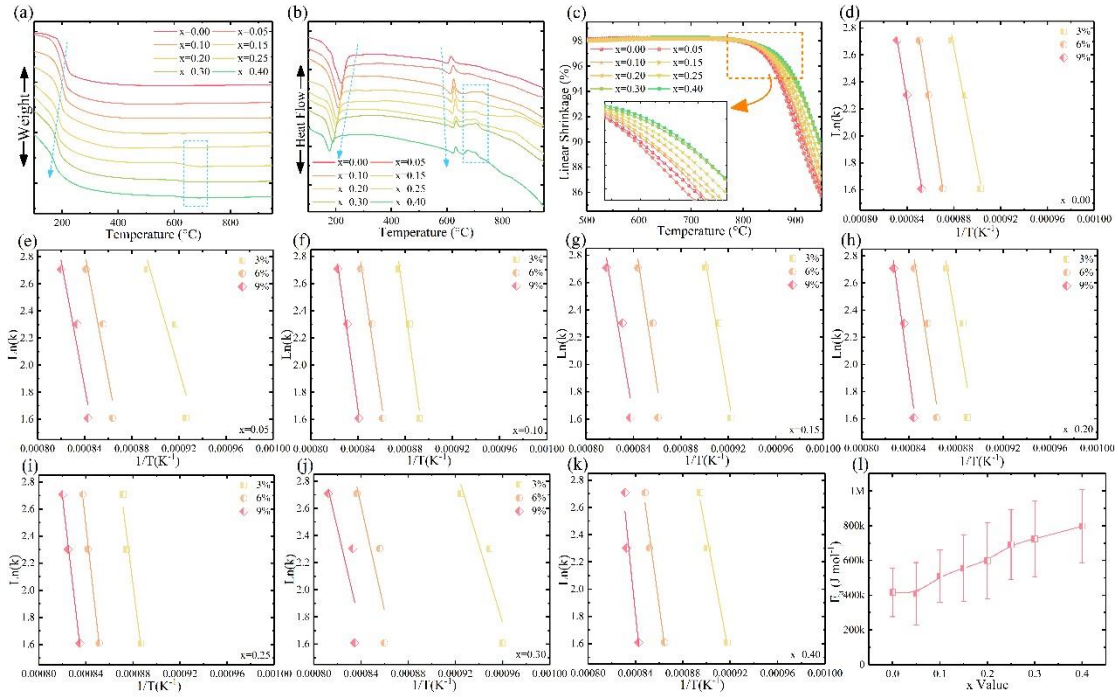

Fig. 6 TG, DSC, TMA and sintering rate plotted against the inverse of temperature of the (1-x)ZBO+xMBO (x=0.00-0.40) ceramics

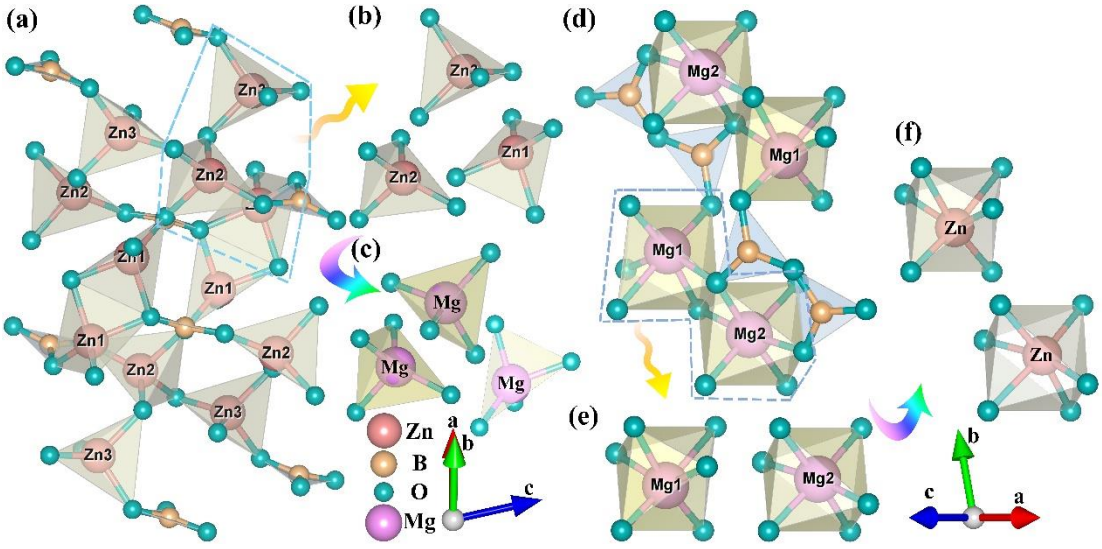

Fig. 7 Crystal structure of ZBO (a); schematic diagram of ZnO_4 tetrahedron before and after Mg^{2+} substitution (b-c); crystal structure of $Mg_2B_2O_5$ (d); schematic diagram of MgO_6 octahedron before and after Zn^{2+} substitution (e-f)

DFT calculations were performed to explain the variation mechanism of sintering and dielectric properties. The crystal structure and schematic diagram of the ion substitution can be observed in Fig. 7. The lattice parameters are *I2/c* (No.15), a=23.406Å, b=5.048Å, c=8.381Å, α=90º, β=97.53º, γ=90º for ZBO, and $P\bar{1}$ (No.2), a=6.187Å, b=9.219Å, c=3.119Å, α=90.4º, β=92.13º, γ=104.32º for $Mg_2B_2O_5$. There are three types of ZnO_4 tetrahedrons in ZBO and two types of MgO_6 octahedrons in $Mg_2B_2O_5$, as illustrated in Fig. 7(b, e). Each zinc/magnesium atom has been substituted by magnesium/zinc atom one by one, and the microstructural properties (electron density, bond length and population) of the atomic groups have been modified after optimization of geometry (Fig. 7(c, f), Fig. 8, Table II). The modification of the position of the ion happened for each ZnO_4 tetrahedron and MgO_6 octahedron. According to the value shown in Table II (Length/Population-B/A means the bond length/population before/after ion substitution, Length-E means the bond length as x=0.2 sintered at 950℃), all the bond length values increased for both the ZnO_4 tetrahedron and the MgO_6 octahedron after substitution. The variation tendency of bond population is negative for ZnO_4 tetrahedron and positive for MgO_6 octahedron. A higher value of bond population corresponds to a higher covalency for the cation and oxygen-ion bond. The variation of bond length and population should be ascribed to the diversity of extranuclear electron pairing status for Zn^{2+} ($3d^{10}$) and Mg^{2+} ($2p^6$), and the difference of ionic polarizability and ionic radius between Zn^{2+} (2.04 $Å^3$) and Mg^{2+} (1.32 $Å^3$) also should be responsible for such variation.[34, 37] It should be noted that the variation of covalency can have an influence on the improvement of the sintering properties, as discussed in the thermal analysis section. The bond lengths (Length-E) obtained from the experiments, the variation trend of it is identical with that of calculation, indicating that all the positions of the zinc and magnesium atoms have participated in the mutual

replacement process, verifying the observations from XRD. The nature of the bonds can be further obtained from the electron density distribution; the (001) plane around the Zn^{2+}/Mg^{2+} is presented in Fig. 8. Compared to the doped and un-doped plane with the ZnO_4 tetrahedron, the electron density has decreased, and the electron interaction between cation and oxygen shows a weakening trend. However, all the variations for the plane containing the MgO_6 octahedron are opposite to that of the ZnO_4 tetrahedron. The electron distribution symmetry in both ZnO_4 tetrahedron and MgO_6 octahedron was broken. This phenomenon can be attributed to the larger polarizability of Zn^{2+} compared to that of Mg^{2+}, and the variation of the bond parameters reflects the changes in the electron distribution. The modification of the electron distribution and bond properties led by mutual substitution are an intrinsic factor for the improvement of the $Q \times f$ value of the composite ceramic.[38]

Table II. Bond length and bond population of ZnO_4 tetrahedron with Mg^{2+} substitution and MgO_6 octahedron with Zn^{2+}-ion substitution; bond length of ZnO_4 tetrahedron and MgO_6 octahedron when x=0.2 sintered at 950℃

Cation	Anion	Length-B (Å)	Length-A (Å)	Length-E (Å)	Population-B	Population-A
Zn1	O14	1.91396	1.97717	1.93546	0.45	-1.38
	O15	1.93280	2.01284	1.96620	0.37	-1.03
	O7	1.96685	2.06893	1.99855	0.37	-0.79
	O1	2.06862	2.07404	2.07058	0.28	-0.89
Zn2	O21	1.91351	1.98619	1.92115	0.44	-1.24
	O4	1.95872	1.99755	1.96074	0.41	-1.17
	O2	1.98725	2.01241	1.99206	0.36	-1.07
	O24	1.99945	2.04499	2.01423	0.35	-0.93
Zn3	O16	1.93785	1.98771	1.95009	0.46	-1.23
	O17	1.95936	1.98718	1.96087	0.39	-1.27
	O18	1.97306	2.03677	1.99233	0.32	-1.01

	O23	1.98923	2.01080	1.99544	0.36	-1.09
Mg1	O2	1.97648	2.00101	1.98221	-2.18	0.58
	O8	2.06725	2.07712	2.07032	-0.95	0.22
	O9	2.16879	2.20867	2.18019	-0.65	0.04
	O10	2.21794	2.26116	2.23021	-0.58	0.30
	O3	2.61087	2.68428	2.64098	-0.65	-0.48
	O4	2.89551	2.94423	2.90469	-0.37	0.50
Mg2	O11	2.04859	2.04929	2.04881	-0.87	0.26
	O1	2.06306	2.09609	2.07585	-1.45	0.44
	O7	2.09595	2.11315	2.10093	-1.14	0.43
	O6	2.14581	2.24873	2.18749	-0.60	0.07
	O5	2.96057	2.98658	2.97014	-0.31	0.46
	O12	2.98457	2.99154	2.98922	-0.34	0.47

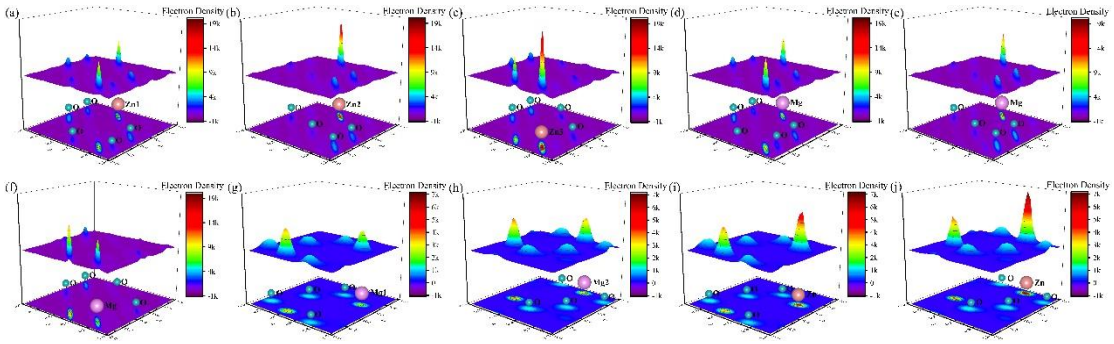

Fig. 8 Electron density map of the plane with three kinds of Zn^{2+} before (a-c) and after (d-f) Mg^{2+} substitution, and the plane with two kinds of Mg^{2+} before (g-h) and after (i-j) Zn^{2+} substitution

In order to further investigate the phase formation property of the (1-x)ZBO+xMBO (x=0.00-0.40) composite ceramics, the formation and total energy of the system have been calculated (chemical potentials are -973.5126eV for Mg, -1710.5005eV for Zn, -7912.8141eV for ZBO, -5712.6593eV for $Mg_3B_2O_6$, -4298.7629eV for $Mg_2B_2O_5$, and -2147.1981eV for ZnO), and the result is presented in

Fig. 9. The formation energy of all doped crystals for the ZBO ceramic is negative, and for the $Mg_2B_2O_5$ ceramic it is positive. The minimum value of formation energy for the doped ZBO system is -4.5116eV (Zn2 site), and the formation energy value of the Mg1 and Mg2 sites is the same. Hence, the ZBO system with the Zn2 site substitution is more stable, and Zn2 site is preferable and more likely to be occupied. The possibility of the Mg1 and Mg2 site to be occupied is equal, and the doping process of Mg^{2+} to the ZBO ceramic is more thermodynamically spontaneous than that of Zn^{2+} to the $Mg_2B_2O_5$ ceramic. The designed and measured total energy/mol for the (1-x)ZBO+xMBO (x=0.00-0.40) composite ceramics were obtained (the formation energy was not considered), as shown in Fig. 9(b). Both the designed and measured total energy/mol show an increasing trend. The former is larger than that of the latter for x=0.05-0.40, and the system with relatively low energy is more stable and spontaneous to form. Hence, for the system with x>0.00, the component fraction discrepancy between the designed and measured sample results from both the larger concentration of Zn^{2+} and lower total energy. These discussions further confirm the XRD refinements.

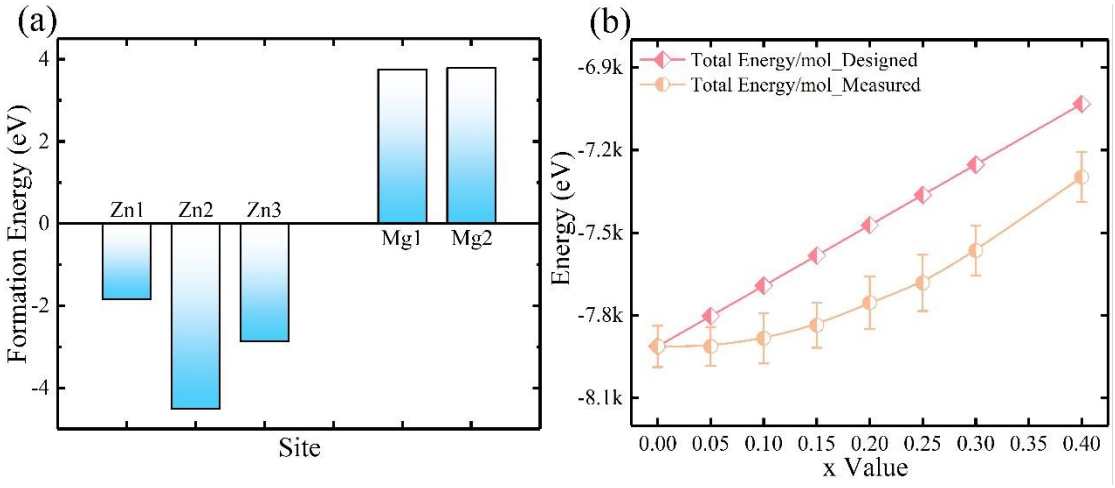

Fig. 9 Formation energy for doped-system of ZBO and $Mg_2B_2O_5$ ceramics (a), designed and measured total energy/mol of the (1-x)ZBO+xMBO (x=0.00-0.40) ceramics

4. Conclusion

The sintering and microwave dielectric properties of the $Zn_3B_2O_6$ ceramic, with a large number of Mg^{2+} substitutions, have been researched profoundly using first principles calculations and solid-state reaction experiment. A solid solution containing three phases ($Zn_3B_2O_6$, $Mg_2B_2O_5$, and ZnO) was formed with mutual substitution (Mg^{2+} and Zn^{2+}). The bond parameters and electron distribution of the ZnO_4 tetrahedron and the MgO_6 octahedron have been modified. The sintering, substitution, and phase formation properties have been analyzed quantitatively through the energy parameters. Peak dielectric properties obtained when the sample with x=0.20 was sintered at 950℃, are ε_r=6.47, $Q\times f$=89,600GHz (15.2GHz), τ_f=-48.6ppm/℃, and relative density=96.7%. The substitution of Mg^{2+} to Zn^{2+} is a feasible method to improve the microwave dielectric properties of the $Zn_3B_2O_6$ ceramic.

Acknowledgements

This work was supported by the Jiangxi Innovative Talent Program, Jiangxi Guochuang & UESTC Joint R & D Center Program (Grant No. H04W190371), and National Natural Science Foundation of China (Grant No. 61771104).

Reference

[1] Y. Lai, X. Tang, X. Huang, H. Zhang, X. Liang, J. Li, H. Su, Phase composition, crystal structure and microwave dielectric properties of Mg2−xCuxSiO4 ceramics, J. Eur. Ceram. Soc. 38 (2018) 1508-1516..

[2] W. Lei, Z. Zou, Z. Chen, B. Ullah, A. Zeb, X. Lan, W. Lu, G. Fan, X. Wang, X. Wang, Controllable τf value of barium silicate microwave dielectric ceramics with different Ba/Si ratios, J. Am. Ceram. Soc. 101 (2018) 25-30.

[3] D. Zhou, C.A. Randall, L. Pang, H. Wang, J. Guo, G. Zhang, X. Wu, L. Shui, X. Yao, Microwave dielectric properties of Li2WO4 ceramic with ultra-low sintering temperature, J. Am. Ceram. Soc. 94 (2011) 348-350.

[4] S. Kweon, M. Joung, J. Kim, B. Kim, S. Nahm, J. Paik, Y. Kim, T. Sung, Low temperature sintering and microwave dielectric properties of B2O3-added LiAlSiO4 ceramics, J. Am. Ceram. Soc. 94 (2011) 1995-1998.
[5] S. Wang, X.B. Zhang, N-doped C@Zn3B2O6 as a low cost and environmentally friendly anode material for Na-ion batteries: high performance and new reaction mechanism, Adv. Mater. 31 (2019) e1805432.
[6] D.G. Chen, W.D. Cheng, D.S. Wu, H. Zhang, Y.C. Zhang, Y.J. Gong, Z.G. Kan, Syntheses, band structures and optical properties of Zn3B2O6 and KZn4B3O9, Solid State Sci. 7 (2005) 179-188.
[7] X. Wu, H. Wang, Y. Chen, D. Zhou, D. Suvorov, Synthesis and microwave dielectric properties of Zn3B2O6 ceramics for substrate application, J. Am. Ceram. Soc. 95 (2012) 1793-1795.
[8] U. Došler, M.M. Kržmanc, B. Jančar, D. Suvorov, A high-Q microwave dielectric material based on Mg3B2O6, J. Am. Ceram. Soc. 93 (2010) 3788-3792.
[9] S. Park, B. Magyari-Köpe, Y. Nishi, Electronic correlation effects in reduced rutile TiO2 within the LDA+U method, Phys. Rev. B 82 (2010).
[10] B.W. Hakki, P.D. Coleman, A dielectric resonator method of measuring inductive capacities in the millimeter range, Ire Trans. Microw. Theory Tech. 8 (2003) 402-410.
[11] C. Zhang, R. Zuo, J. Zhang, Y. Wang, J. Jones, Structure-dependent microwave dielectric properties and middle-temperature sintering of forsterite (Mg1-xNix)2SiO4 ceramics, J. Am. Ceram. Soc. 98 (2015) 702-710.
[12] H. Zhuang, Z. Yue, F. Zhao, J. Pei, L. Li, Microstructure and microwave dielectric properties of Ba5Nb4O15–BaWO4 composite ceramics, J. Alloy. Compd. 472 (2009) 411-415.
[13] Y. Lv, R. Zuo, Y. Cheng, C. Zhang, P. Davies, Low-temperature sinterable (1−x)Ba3(VO4)2-xLiMg0.9Zn0.1PO4 microwave dielectric ceramics, J. Am. Ceram. Soc. 96 (2013) 3862-3867.
[14] Y. Wang, Y. Chen, S. Yao, C. Wu, Microwave dielectric properties of neodymium tin oxide, Ceram. Int. 40 (2014) 2641-2645.
[15] H. Yang, E. Li, S. Duan, H. He, S. Zhang, Structure, microwave properties and low temperature sintering of Ta2O5 and Co2O3 codoped Zn0.5Ti0.5NbO4 ceramics, Mater. Chem. Phys. 199 (2017) 43-53.
[16] M. Valant, D. Suvorov, R.C. Pullar, K. Sarma, N.M. Alford, A mechanism for low-temperature sintering, J. Eur. Ceram. Soc. 26 (2006) 2777-2783.
[17] D. Zhou, F. Sun, Y. Hu, Q. Fu, G. Dou, Low-temperature sintering and microwave dielectric properties of Mg3B2O6-LMZBS composites, J. Mater. Sci-Mater. El. 23 (2011) 981-989.
[18] G. Dou, M. Guo, Y. Li, J. Lin, The effect of LMBS glass on the microwave dielectric properties of the Mg3B2O6 for LTCC, J. Mater. Sci-Mater. El. 26 (2015) 4207-4211.
[19] U. Došler, M.M. Kržmanc, D. Suvorov, The synthesis and microwave dielectric properties of Mg3B2O6 and Mg2B2O5 ceramics, J. Eur. Ceram. Soc. 30 (2010) 413-418.
[20] M. Kim, J. Lim, J. Kim, S. Nahm, J. Paik, J. Kim, K. Park, Synthesis of BaCu(B2O5) ceramics and their effect on the sintering temperature and microwave dielectric properties of Ba(Zn1/3Nb2/3)O3 ceramics, J. Am. Ceram. Soc. 89 (2006) 3124-3128.
[21] M. Ohashi, H. Ogawa, A. Kan, E. Tanaka, Microwave dielectric properties of low-temperature sintered Li3AlB2O6 ceramic, J. Eur. Ceram. Soc. 25 (2005) 2877-2881.
[22] X. Chen, W. Zhang, B. Zalinska, I. Sterianou, S. Bai, I.M. Reaney, C.A. Randall, Low sintering temperature microwave dielectric ceramics and composites based on Bi2O3-B2O3, J. Am. Ceram. Soc.

95 (2012) 3207-3213.
[23] R. Peng, Y. Lu, Z. Tao, D. Chen, L. Shi, Q. Zhang, Y. Li, Improved microwave dielectric properties and sintering behavior of LiZnPO4 ceramic by Ni2+-ion doping based on first-principle calculation and experiment, Ceram. Int. 46 (2020) 11021-11032.
[24] R. Peng, Y. Li, G. Yu, Y. Lu, S. Li, Effect of Co2+ substitution on the microwave dielectric properties of LiZnPO4 ceramics, J. Electron. Mater. 47 (2018) 7281-7287.
[25] R. Peng, Y. Li, H. Su, Y. Lu, Y. Yun, Q. Zhang, S. Zhang, Effect of cobalt-doping on the dielectric properties and densification temperature of Li2MgSiO4 ceramic: calculation and experiment, J. Alloy. Compd. 827 (2020) 154162.
[26] D. Thomas, M.T. Sebastian, Temperature-compensated LiMgPO4: a new glass-free low-temperature cofired ceramic, J. Am. Ceram. Soc. 93 (2010) 3828-3831.
[27] R. Peng, H. Su, D. An, Y. Lu, Z. Tao, D. Chen, L. Shi, Y. Li, The sintering and dielectric properties modification of Li2MgSiO4 ceramic with Ni2+-ion doping based on calculation and experiment, J. Mater. Res. Technol. 9 (2020) 1344-1356.
[28] Z. Cheng, X. Hu, Y. Li, Z. Ling, N. Alford, Fabrication and microwave dielectric properties of Mg2SiO4-LiMgPO4-TiO2 composite ceramics, J. Am. Ceram. Soc. 99 (2016) 2688-2692.
[29] G. Dou, D. Zhou, S. Gong, M. Guo, Low temperature sintering and microwave dielectric properties of Li2ZnSiO4 ceramics with ZB glass, J. Mater. Sci-Mater. El. 24 (2012) 1601-1607.
[30] T.S. Sasikala, C. Pavithran, M.T. Sebastian, Effect of lithium magnesium zinc borosilicate glass addition on densification temperature and dielectric properties of Mg2SiO4 ceramics, J. Mater. Sci-Mater. El. 21 (2009) 141-144.
[31] R. Umemura, H. Ogawa, H. Ohsato, A. Kan, A. Yokoi, Microwave dielectric properties of low-temperature sintered Mg3(VO4)2 ceramic, J. Eur. Ceram. Soc. 25 (2005) 2865-2870.
[32] R. Peng, Y. Li, Y. Lu, Y. Yun, W. Du, Z. Tao, B. Liao, High-performance microwave dielectric composite ceramics sintered at low temperature without sintering-aids, J. Alloy. Compd. 831 (2020) 154878.
[33] M. Guo, Y. Li, G. Dou, J. Lin, A new microwave dielectric ceramics for LTCC applications: Li2Mg2(WO4)3 ceramics, J. Mater. Sci-Mater. El. 25 (2014) 3712-3715.
[34] R.D. Shannon, Dielectric polarizabilities of ions in oxides and fluorides, J. Appl. Phys. 73 (1993) 348-366.
[35] G. Gouadec, P. Colomban, Raman Spectroscopy of nanomaterials: How spectra relate to disorder, particle size and mechanical properties, Prog. Cryst. Growth Ch. 53 (2007) 1-56.
[36] E.A. Barringer, The synthesis, interfacial electrochemistry, ordering, and sintering of monodisperse TiO2 powders, Massachusetts Institute of Technology, 1983.
[37] R. Lacomba, J. Ruiz, D. Errandonea, D. Martínez, A. Segura, Optical absorption of divalent metal tungstates: Correlation between the band-gap energy and the cation ionic radius, Europhys. Lett. 83 (2008) 37002.
[38] V.L. Gurevich, A.K. Tagantsev, Intrinsic dielectric loss in crystals, Adv. Phys. 40 (1991) 719-767.